Limestone conversion to cement clinker precursor in a zero-gap electrolyzer

Tengxiao Ji[1†], Shaoxuan Ren[1†], Gaopeng Jiang[1], Yumeng Yang[2], Siwei Ma[1], Christopher E. B. Waizenegger[1], Yongwook Kim[1], Andrew M. L. Jewlal[1], Monika Stolar[1], and Curtis P. Berlinguette[1,2,3,4,*]

[1]Department of Chemistry, The University of British Columbia, 2036 Main Mall, Vancouver, British Columbia, V6T 1Z1, Canada.

[2]Department of Chemical and Biological Engineering, The University of British Columbia, 2360 East Mall, Vancouver, British Columbia, V6T 1Z3, Canada.

[3]Stewart Blusson Quantum Matter Institute, The University of British Columbia, 2355 East Mall, Vancouver, British Columbia, V6T 1Z4, Canada.

[4]Canadian Institute for Advanced Research (CIFAR), 661 University Avenue, Toronto, Ontario, M5G 1M1, Canada.

†These authors contributed equally to this work.

Correspondence: cberling@chem.ubc.ca

https://doi.org/10.26434/chemrxiv-2024-fvxrb **ORCID:** https://orcid.org/0000-0001-6875-849X Content not peer-reviewed by ChemRxiv. **License:** CC BY-NC-ND 4.0

Abstract

The carbon intensity of industrial cement production could be reduced if the high-temperature kilns used to decompose limestone ($CaCO_{3(s)}$) were replaced. One possible solution is to use electrochemical reactors to convert $CaCO_{3(s)}$ into $Ca(OH)_{2(s)}$. The challenge is that the continuous-flow electrochemical reactors reported to date all require voltages that are too high (>4 V at 100 mA cm^{-2}) to be put into practice. A key reason for these high voltages is that the reactors contain a chemical chamber, inserted between the anode and cathode chambers, that leads to a high Ohmic resistance. In this study, we present an electrolyzer that decomposes $CaCO_{3(s)}$ into reactive Ca^{2+} ions using only two chambers. This cell design, with an anode and cathode chamber separated by a membrane instead of a chemical chamber, follows a "zero-gap" design akin to hydrogen-producing electrolyzers and fuel cells. This cement electrolyzer is capable of operating at a full cell voltage (E_{cell}) of merely 0.38 V at 100 mA cm^{-2}, and with 100% faradaic efficiency (FE). This strikingly low E_{cell} is 1.4 V lower than any other reported E_{cell}. We achieved this goal by not only eliminating the chemical chamber, but by also engaging the reversible redox activity of (hydro)anthraquinones to mediate oxidation and reduction within a narrow electrochemical window. This streamlined reactor is capable of operating at a record low voltages of 0.38 V at 100 mA cm^{-2}, and 4.23 V at 1 A cm^{-2}.

One sentence summary: A zero-gap 2-chamber electrolyzer demonstrated successful $Ca(OH)_{2(s)}$ production at 0.38 V and 100 mA cm^{-2}.

https://doi.org/10.26434/chemrxiv-2024-fvxrb **ORCID:** https://orcid.org/0000-0001-6875-849X Content not peer-reviewed by ChemRxiv. **License:** CC BY-NC-ND 4.0

The cement industry accounts for 8% of global CO_2 emissions.(*1–3*) The carbon intensity of cement production arises from the combustion of fossil fuels needed to reach the high temperatures (>900 ºC) needed to decompose limestone ($CaCO_{3(s)}$). This decomposition process also releases stoichiometric amounts of $CO_{2(g)}$ from limestone (Eq. 1) before the $CaO_{(s)}$ is converted into cement clinker (Eq. 2). Several methods are being considered to lower the carbon intensity of cement production, including the sequestration of CO_2 within concrete,(*4*, *5*) the replacement of limestone with calcium-bearing silicate rock,(*6*, *7*) and the use of electric ovens to thermally drive limestone decomposition.(*2*, *8–10*)

Limestone calcination	$CaCO_{3(s)} \rightarrow CaO_{(s)} + CO_{2(g)}$	Eq. 1
Clinker formation	$CaO_{(s)} + SiO_{2(s)} \rightarrow 3CaO \cdot SiO_{2(s)}$	Eq. 2

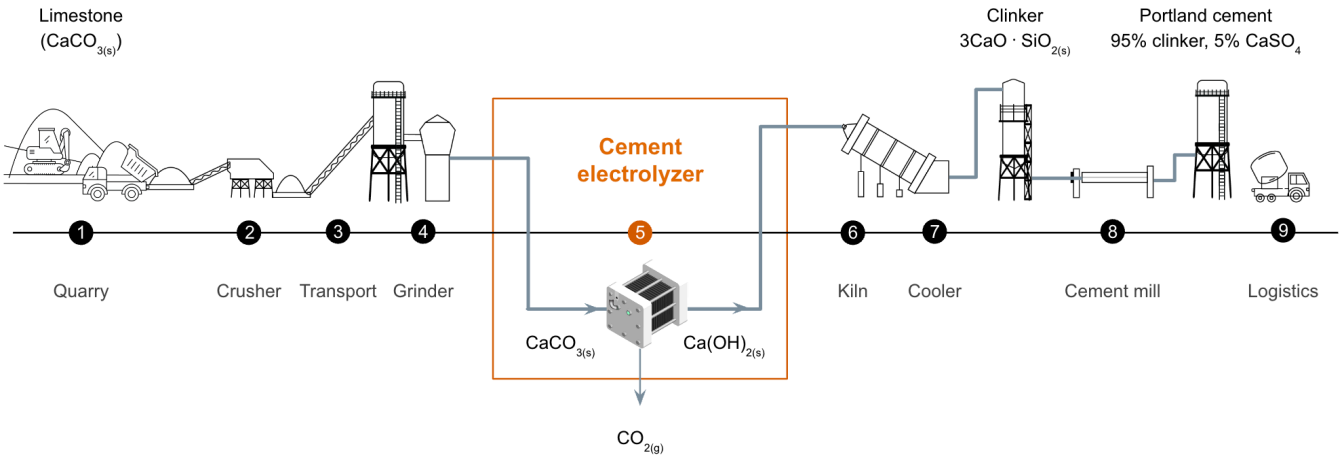

Fig. 1: Thermal and electrochemical cement production. Industrial cement production involves the grinding and thermal decomposition of limestone ($CaCO_{3(s)}$) in a precalciner at >900 °C to form $CaO_{(s)}$ and $CO_{2(g)}$. The $CaO_{(s)}$ is then heated with $SiO_{2(s)}$ in a kiln set at >1400 ºC to form cement clinker precursor ($Ca(OH)_{2(s)}$). A cement electrolyzer electrochemically generates acid to decompose $CaCO_{3(s)}$ into Ca^{2+} ions, and then converts Ca^{2+} into $Ca(OH)_{2(s)}$. This solid can then be heated with $SiO_{2(s)}$ in a kiln set at >1400 ºC to form cement clinker precursors. The $CO_{2(g)}$ released from the cement electrolyzer can then be upgraded or stored.

https://doi.org/10.26434/chemrxiv-2024-fvxrb **ORCID:** https://orcid.org/0000-0001-6875-849X Content not peer-reviewed by ChemRxiv. **License:** CC BY-NC-ND 4.0

Another pathway for decarbonizing cement production is to electrochemically produce cement clinker precursor ($Ca(OH)_{2(s)}$) using renewable electricity (Fig. 1).(*2*, *8*) We previously demonstrated a continuous flow three-chamber electrochemical reactor that electrolytically produces H^+ ions, sourced from water, at an anode that react with $CaCO_{3(s)}$ to form Ca^{2+} ions in a chemical chamber, which, in turn, react with OH^- formed at the cathode to form $Ca(OH)_{2(s)}$ (Fig. 2).(*8*) The challenge with this electrolyzer is that the voltage (>4 V at 100 mA cm^2) needed to drive the reaction is too high to be practical.(*2*, *8*, *10–13*) Cement electrolyzers will need to operate at a cell voltage (E_{cell}) below 1.5 V and at current densities greater than 100 mA cm^{-2} to compete with how cement is produced commercially today (fig. S1).

We therefore sought alternative ways to lower the voltage required to electrochemically drive the production of cement clinker precursor. We focused our attention on addressing three aspects of the cement electrolyzer that contribute to the high voltages: (i) the inherently high ohmic resistance associated with using a chemical chamber in between the anode and cathode chambers; (ii) the high potentials needed to generate H^+ from water at the anode (oxygen evolution reaction, OER; E^0 = 1.23 V vs NHE at pH = 0); and (iii) the high potentials needed to drive water dissociation at a bipolar membrane (BPM; E^0 = 0.83 V). Here, we engage the proton-coupled electron transfer (PCET) chemistry(*14*) associated with a quinone-based redox-active electrolyte to create a two-chamber, zero-gap electrolyzer that converts $CaCO_{3(s)}$ into $Ca(OH)_{2(s)}$.

https://doi.org/10.26434/chemrxiv-2024-fvxrb **ORCID:** https://orcid.org/0000-0001-6875-849X Content not peer-reviewed by ChemRxiv. **License:** CC BY-NC-ND 4.0

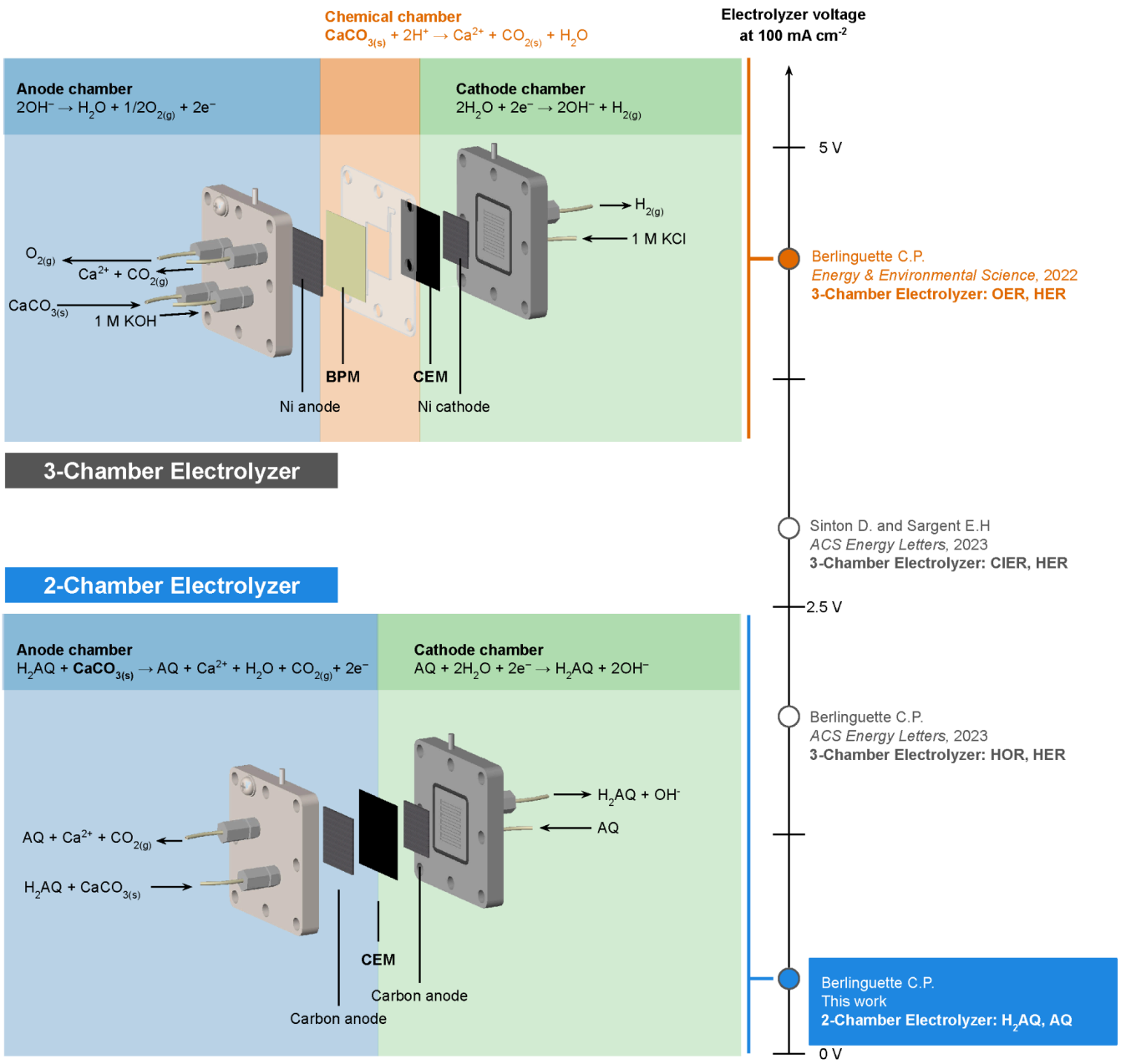

Fig. 2: Benchmarked operating voltages of electrochemical cement electrolyzers at 100 mA/cm^2. Expanded view illustrations of our initial three-chamber cement electrolyzer ("Control Electrolyzer") and the two-chamber cement electrolyzer reported here ("2-Chamber Electrolyzer").(*8*, *9*, *13*) The key reaction chemistries that occur within each chamber is indicated. (OER: oxygen evolution reaction; HER: hydrogen evolution reaction; ClER: chloride electrochemical oxidation reaction; HOR: hydrogen oxidation reaction)

https://doi.org/10.26434/chemrxiv-2024-fvxrb ORCID: https://orcid.org/0000-0001-6875-849X Content not peer-reviewed by ChemRxiv. License: CC BY-NC-ND 4.0

An enabling feature of the updated cement electrolyzer is the use of an anolyte and catholyte containing a (hydro)anthraquinone redox shuttle [i.e., dihydroanthraquinone-2,7-disulfonic acid disodium salt (H_2AQ) and anthraquinone-2,7-disulfonic acid disodium salt (AQ)]. The H_2AQ species can be oxidized (–0.25 V vs NHE at pH 7.5) at a lower potential than OH^- (E_{OER} = 1.7 V vs NHE at pH 7.5),(*15*) thereby reducing the voltage required to generate acid at the anode. The AQ species is reduced at a potential (–0.46 V vs NHE at pH 7.5) slightly favorable to HER that occurs in our system starting at –1.4 V vs NHE at pH 7.5.(*15*) Consequently, AQ requires a lower voltage to form hydroxide at the cathode. Consequently, the oxidation and reduction of H_2AQ and AQ, respectively, occurs within a narrow electrochemical window within water oxidation and reduction (fig. S2).

The voltage of the three-chamber cement electrolyzer that we previously reported ("Control Electrolyzer") can therefore be reduced from 4.55 V to 1.95 V at 100 mA cm^{-2} by using $(H_2)AQ$ as the anolyte and catholyte ("3-Chamber Electrolyzer"; fig. S3). We lowered the voltage further by (i) replacing the BPM used in the 3-Chamber Electrolyzer with a cation exchange membrane (CEM), and (ii) removing the middle chemical chamber to form a two-chamber electrolyzer configuration. This simplified zero-gap, two-chamber electrolyzer ("2-Chamber Electrolyzer"; Fig. 2) yields a record low voltage of 1.31 V at 100 mA cm^{-2} at 20 ℃ in aqueous media. This voltage was lowered further to 0.38 V (Fig. 2) by using a water/acetonitrile (H_2O/MeCN, 4:1) mixed-electrolyte system, and with operation at an elevated temperature of 60 ℃. These conditions also benefited the $Ca(OH)_{2(s)}$ production by suppressing the formation of quinone dimer byproducts at the anode, and by increasing the pH of the catholyte to increase the formation of the desired $Ca(OH)_{2(s)}$ upon combination with the anolyte containing Ca^{2+} in a secondary reactor ("Calcium Reactor").

These collective design changes present a new pathway for potentially decarbonizing cement production, and showcase yet another example of how redox-active quinones can be utilized for energy-related applications.(*16–24*)

https://doi.org/10.26434/chemrxiv-2024-fvxrb **ORCID:** https://orcid.org/0000-0001-6875-849X Content not peer-reviewed by ChemRxiv. **License:** CC BY-NC-ND 4.0

For this study, we designed, built, and tested three different electrolyzer configurations that we denote herein as the Control Electrolyzer, 3-Chamber Electrolyzer, and 2-Chamber Electrolyzer (Table 1). The experiments were designed to electrolytically produce H^+, convert limestone into Ca^{2+} ions, and to produce OH^- under continuous flow in the electrochemical reactors. The Ca^{2+} ions and OH^- were then mixed in a batch process within a separate Calcium Reactor.

Table 1. Summary of Differentiated Features of the Three Electrolyzers Tested in this Study.

	Control Electrolyzer	3-Chamber Electrolyzer	2-Chamber Electrolyzer
Number of chambers	3	3	2
Membrane(s)	BPM, CEM	BPM, CEM	CEM
Anode reaction	$2OH^- \rightarrow 1/2O_{2(g)} + H_2O + 2e^-$	$H_2AQ \rightarrow AQ + 2H^+ + 2e^-$	$H_2AQ + CaCO_{3(s)} \rightarrow$ $AQ + Ca^{2+} + CO_{2(g)} + H_2O + 2e^-$
Cathode reaction	$2H_2O + 2e^- \rightarrow H_{2(g)} + 2OH^-$	$AQ + H_2O + 2e^- \rightarrow H_2AQ + 2OH^-$	$AQ + H_2O + 2e^- \rightarrow H_2AQ + 2OH^-$

Each experimental campaign consisted of three iterative phases (Fig. 3). During Phase 1, electrolysis was performed for at least 30 minutes while recirculating the same electrolyte through each of the anode and cathode chambers. Because the anolyte and catholyte were not mixed during the electrolysis experiments, the concentrations of Ca^{2+} and AQ would build up with time in the anolyte, while H_2AQ and OH^- formed with time in the catholyte. Electrolysis was then stopped. Phase 2 involved manually stirring the Ca^{2+}-enriched anolyte and the OH^--enriched catholyte in an independent round bottom flask (Calcium Reactor) to precipitate $Ca(OH)_{2(s)}$ (Fig 3). For Phase 3, the $Ca(OH)_{2(s)}$ product was isolated, and resultant electrolyte solution was then reused for electrolysis experiments. Half of the solution was used as the anolyte, the other half as the catholyte. Phase 1, 2 and 3 were then repeated in succession. Each repeat is denoted a "Cycle". The experimental campaign reported here was performed for at least 4 cycles.

https://doi.org/10.26434/chemrxiv-2024-fvxrb ORCID: https://orcid.org/0000-0001-6875-849X Content not peer-reviewed by ChemRxiv. License: CC BY-NC-ND 4.0

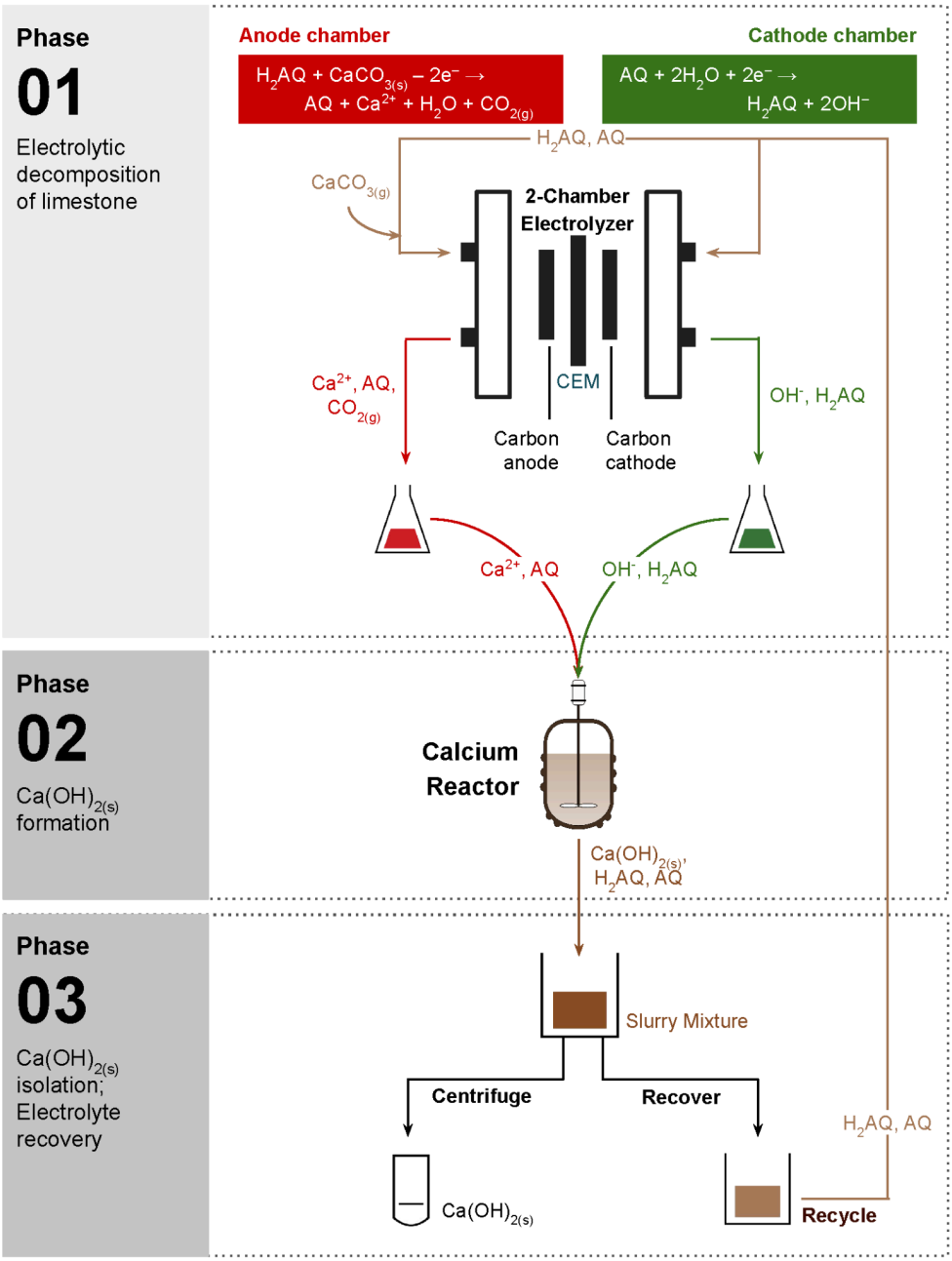

Fig. 3: Schematic description of experimental streamline for 2-Chamber Electrolyzer. The electrochemical reaction was first performed to dissolve $CaCO_{3(s)}$ and produce OH^- (Phase 1). The electrolytes were mixed to precipitate $Ca(OH)_{2(s)}$ in a Calcium Reactor (Phase 2). Finally, the $Ca(OH)_{2(s)}$ was isolated and the electrolyte was reused.

A convenient feature of the experiments is that the H_2AQ, AQ, and $Ca(OH)_{2(s)}$ are distinctively red, green, and white, respectively. These distinctive colors help inform the chemical species occurring in the electrolyzers and the Calcium Reactor.

https://doi.org/10.26434/chemrxiv-2024-fvxrb ORCID: https://orcid.org/0000-0001-6875-849X Content not peer-reviewed by ChemRxiv. License: CC BY-NC-ND 4.0

Electrolyzer configurations

The Control Electrolyzer was the same as we previously reported.(*8*) Nickel foam was used for both the anode and cathode, each with an active area 5 cm^2. This electrolyzer relies on the OER in the anode chamber (Eq. 3; Fig. 2 and Table 1), using a 1 M KOH.(*12*) A BPM separates the anode chamber from an adjacent chemical chamber, and a CEM coated with Ca^{2+}-blocking polyaniline separates the chemical chamber from the cathode chamber.(*12*) The protons generated from water dissociation (Eq. 4) within the BPM enter the chemical chamber to react with $CaCO_{3(s)}$ (Eq. 5). The $CaCO_{3(s)}$ was delivered to the chemical chamber as an aqueous slurry of microparticles (20 g L^{-1}) in 1 M KCl. A 1 M KCl solution catholyte was delivered to the cathode chamber, where HER occurs at the cathode. The flow rates for all three electrolytes entering the electrolyzer were set to 150 mL min^{-1}. This flow rate was used for all the electrolyzers.

Anode chamber (OER)	$2OH^- \rightarrow H_2O + 1/2O_{2(g)} + 2e^-$	Eq. 3
BPM	$2H_2O \rightarrow 2OH^- + 2H^+$	Eq. 4
Chemical chamber	$CaCO_{3(s)} + 2H^+ \rightarrow Ca^{2+} + CO_{2(g)} + H_2O$	Eq. 5
Cathode chamber (HER)	$2H_2O + 2e^- \rightarrow 2OH^- + H_{2(g)}$	Eq. 6
Overall reaction	$CaCO_{3(s)} + H_2O \rightarrow Ca(OH)_{2(s)} + CO_{2(g)}$	Eq. 7

The 3-Chamber Electrolyzer followed the same design as the Control Electrolyzer, except that (i) 0.2 M $(H_2)AQ$ (1:1, 0.1 M H_2AQ and 0.1 M AQ) in 1 M potassium acetate (KOAc) was used as the anolyte and catholyte, respectively, and (ii) graphite felt was used as both electrodes. The reaction that occurs at the anode is H_2AQ oxidation (Eq. 8; fig. S3), and at the cathode is AQ reduction (Eq. 9).

Anode chamber (PCET)	$H_2AQ \rightarrow AQ + 2H^+ + 2e^-$	Eq. 8
Cathode chamber (PCET)	$AQ + 2H_2O + 2e^- \rightarrow H_2AQ + 2OH^-$	Eq. 9

https://doi.org/10.26434/chemrxiv-2024-fvxrb **ORCID:** https://orcid.org/0000-0001-6875-849X Content not peer-reviewed by ChemRxiv. **License:** CC BY-NC-ND 4.0

The 2-Chamber Electrolyzer was designed without a chemical chamber between the anode and cathode chambers (Fig. 2 and Table 1). The anode and cathode chambers were separated instead by a Ca^{2+}-blocking CEM. This configuration was designed so that H^+ generated by H_2AQ oxidation react with $CaCO_{3(s)}$ suspended in the anolyte (H_2AQ in 1 M KOAc) to form Ca^{2+} and $CO_{2(g)}$ (i-$CO_{2(g)}$, Eq. 10). The i-$CO_{2(g)}$ was quantified by purging N_2 (200 sccm) through the anolyte to an in-line gas chromatograph (GC) after 5 min of electrolysis. Notably, this design change also resulted in a zero-gap electrolyzer configuration,(*25*, *26*) where the anode and cathode are pressed tightly against the membrane.

Anode chamber (PCET) $$H_2AQ + CaCO_{3(s)} \rightarrow AQ + Ca^{2+} + CO_{2(g)} + H_2O + 2e^- \quad \text{Eq. 10}$$

All three reactors used a polyaniline-coated CEM to block the diffusion of Ca^{2+} through the membrane. To test the efficacy of this membrane for blocking Ca^{2+}, we quantified the amount of Ca^{2+} ions in the anolyte and catholyte by inductively-coupled plasma optical emission spectroscopy (ICP-OES) for the 2-Chamber Electrolyzer. After 120 min (4 Cycles) of electrolysis at 100 mA cm^{-2}, 0.3 ppm of Ca^{2+} was detected in the catholyte. We took this result to indicate that >98.9% of Ca^{2+} ions were prevented from crossing the membrane into the catholyte over the course of each experiment.

Cement electrolysis experiments

We ran experimental campaigns with each of the three electrolyzers where electrolysis was performed at 100 mA cm^{-2} and 20 ºC for 30 min, unless stated otherwise. We recorded an E_{cell} of 4.6 V for the Control Electrolyzer, consistent with our previous reported paper.(*9*, *12*) We measured an E_{cell} of 2.0 V and 1.3 V at 100 mA cm^{-2} for 3-Chamber Electrolyzer and 2-Chamber Electrolyzer, respectively, and 13.0 V and 8.1 V at 1 A cm^{-2} (Fig. 4a, fig. S4, and Table 2).

https://doi.org/10.26434/chemrxiv-2024-fvxrb **ORCID:** https://orcid.org/0000-0001-6875-849X Content not peer-reviewed by ChemRxiv. **License:** CC BY-NC-ND 4.0

Table 2. Cell Voltages Required to Drive Electrolysis at 100 and 1000 mA cm^{-2}. All reported voltages are those measured at 5 min during Cycle 1.[a]

J (mA cm^{-2})	Full cell voltage (V)		
	Control Electrolyzer	3-Chamber Electrolyzer	2-Chamber Electrolyzer
100	4.6	2.0	1.3 (0.3[b]; 0.4[c])
1000	16.4	13.1	8.1 (5.0[b]; 4.2[c])

[a] Data recorded at an aqueous electrolyte temperature of 20 ºC. [b] Data recorded at an aqueous electrolyte temperature of 60 ºC. [c] Data recorded at an H_2O/MeCN (4:1 *v:v*) electrolyte temperature of 60 ºC.

The voltages for each of the electrolyzers did not stay constant over the course of the electrolysis experiments, largely due to the build up of ions during electrolysis. Notwithstanding, the drift in voltage was not as significant for 2-Chamber Electrolyzer as it was for the three-chamber electrolyzers: The voltage increased by 0.3 V for 2-Chamber Electrolyzer over 30 minutes of electrolysis at 100 mA cm^{-2} (Fig. 6), and by >1 V within 18 min of electrolysis in Control Electrolyzer and 3-Chamber Electrolyzer.

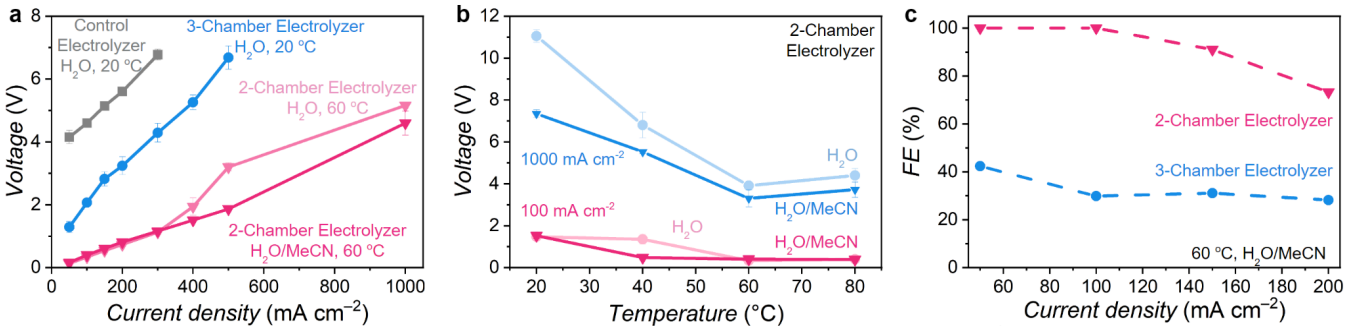

Fig. 4: Cell voltage profiles for each of the three electrolyzers. a Voltage measured as a function of current density using aqueous or H_2O/MeCN (4:1) mixed electrolytes set at 60 ºC for the 2-Chamber Electolyzer. The Control and 3-Chamber Electrolyzers use aqueous electrolytes at 20 ºC. **b** Voltage measured as a function of electrolyte temperature for electrolysis experiments performed at 100 (pink) or 1000 (blue) mA cm^{-2} using either an aqueous or H_2O/MeCN electrolyte. **c** Calculated Faradaic efficiency (FE) of *i*-$CO_{2(g)}$ from the anode chamber in a 2-Chamber Electrolyzer (pink) and the chemical chamber in a 3-Chamber Electrolyzer (blue) after 5 min of reaction at 100 mA cm^{-2}.

While all the electrolyzers are continuous flow reactors, the electrolyzers were not coupled to the Calcium Reactor to minimize complexity. As such, the precipitation of $Ca(OH)_{2(s)}$ was carried out as a

https://doi.org/10.26434/chemrxiv-2024-fvxrb ORCID: https://orcid.org/0000-0001-6875-849X Content not peer-reviewed by ChemRxiv. License: CC BY-NC-ND 4.0

batch process in the Calcium Reactor, and the filtrate (i.e., the electrolyte) was then reused for a successive Cycle. The E_{cell} increased by <0.2 V over 4 electrolyte recycling cycles for each of the electrolyzers (Fig. 5b).

For these experiments, we measured a Faradaic efficiency (FE) of 100% for i-$CO_{2(g)}$ generation for 2-Chamber Electrolyzer (Fig. 4c and fig. S5), a surrogate indicator of all electrochemically generated H^+ reacting with $CaCO_{3(s)}$. The FE was merely 30% for 3-Chamber Electrolyzer. Supplementary Video 1 qualitatively support these measurements by showing a higher amount of i-$CO_{2(g)}$ being generated in 2-Chamber Electrolyzer, where i-$CO_{2(g)}$ bubbles adhere to and bring the $CaCO_{3(s)}$ microparticles to the surface of the anolyte slurry.

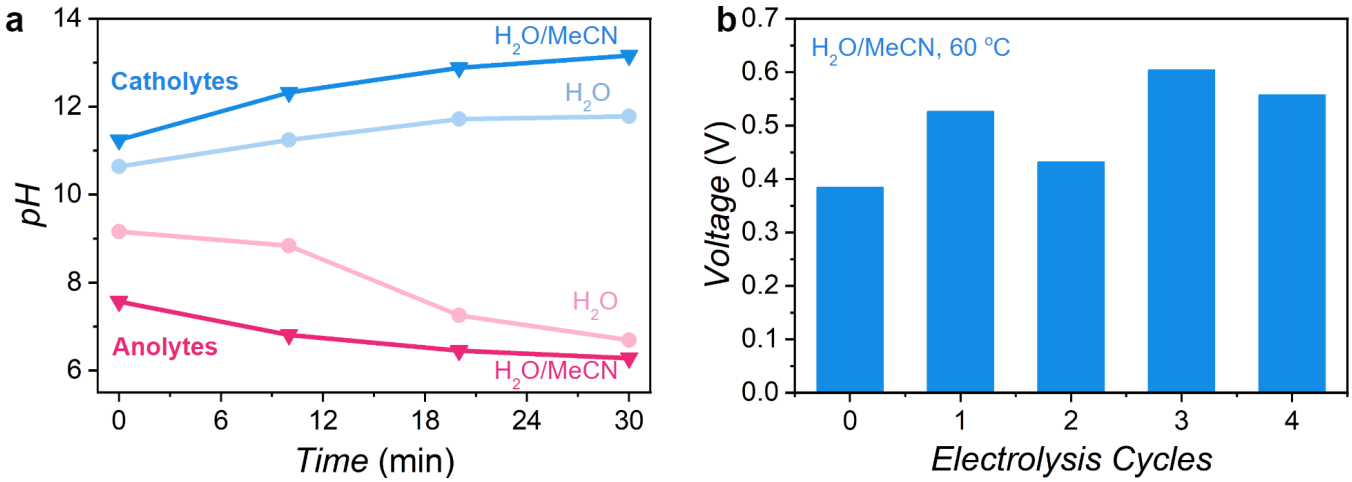

Fig. 5: Electrochemical performance and product characterization of 2-Chamber Electrolyzer with H_2O/MeCN (4:1) mixed electrolyte at 60 ℃. a Tracked pH changes in the electrolytes over a 30 min reaction campaign. **b** Voltage measured on 2-Chamber Electrolyzer after 5 min of electrolysis during Phase 2 for five successive Cycles. The same electrolyte was used for all Cycles.

Identification of solid byproducts in the anode chamber

We encountered the challenge of solid byproduct formation at the anode during electrolysis at room temperature using 2-Chamber Electrolyzer. Specifically, a dark precipitate would form along the flow channels at the graphite felt surface (fig. S6). The formation of this precipitate was commensurate with increases in anode resistances and cell voltages during electrolysis (Fig. 6).

https://doi.org/10.26434/chemrxiv-2024-fvxrb ORCID: https://orcid.org/0000-0001-6875-849X Content not peer-reviewed by ChemRxiv. License: CC BY-NC-ND 4.0

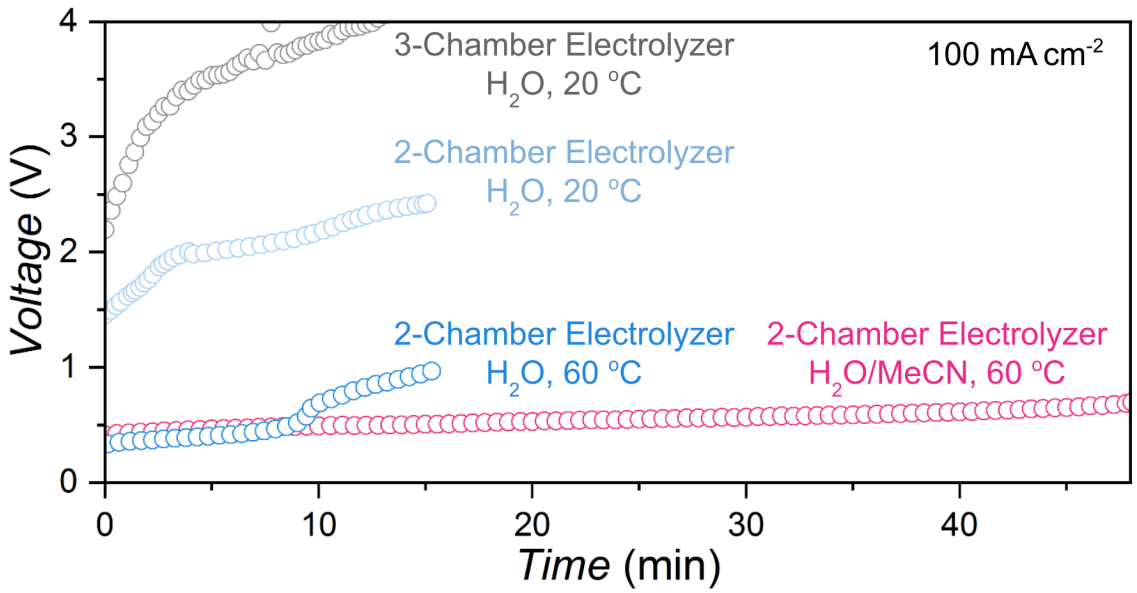

Fig. 6 Electrolyzer voltages recorded as a function of time at 100 mA cm^{-2}. The flow rate of the (H_2)AQ electrolytes was slowed to 100 mL min^{-1} to reduce the deformation of the CEM in long-term experiment. (Reaction conditions: gray, 3-Chamber Electrolyzer, solvent: H_2O at 20 ºC; blue, 2-Chamber Electrolyzer, solvent, H_2O at 60ºC; pink, 2-Chamber Electrolyzer, H_2O/MeCN (4:1) at 60 ºC)

These solid byproducts were deemed to be dimers of the quinone species based on analysis with scanning electron microscopy with energy dispersive X-ray spectroscopy (EDX; fig. S7), ultraviolet–visible (UV-vis) spectroscopy (fig. S8), ^{1}H NMR (fig. S9), and mass spectrometry (MS, fig. S10).(*27*) At elevated temperatures >60 °C, the formation of byproducts was not observed on the electrode surface, and the voltage readings remained relatively constant during electrolysis (Fig. 6).

Temperature-dependent electrolysis experiments

To address the aforementioned solid byproduct formation, we ran experimental campaigns with the electrolyte at progressively higher temperature using 2-Chamber Electrolyzer. When the temperature was increased from 20 to 60 ºC, the E_{cell} was reduced from 1.31 V to 0.32 V at 100 mA cm^{-2}, and from 11.44 V to 5.03 V at 1 A cm^{-2} (Fig. 4a). A further voltage improvement was not observed at the higher temperature of 80 ºC (fig. S4 and table S1).

https://doi.org/10.26434/chemrxiv-2024-fvxrb ORCID: https://orcid.org/0000-0001-6875-849X Content not peer-reviewed by ChemRxiv. License: CC BY-NC-ND 4.0

We hypothesized that the decrease in E_{cell} was due to improved diffusion of $(H_2)AQ$ molecules. To validate this hypothesis, we determined the diffusion coefficient by performing cyclic voltammetry measurements on aqueous $(H_2)AQ$ (1:1) electrolyte (fig. S11, tables S2 and S3). This analysis showed that the diffusion coefficient increased from 2.5×10^{-4} to 6.09×10^{-4} cm^2 s^{-1} when heating the electrolyte from 20 ºC to 60 ºC.

Electrolyte engineering

We set out to further improve the electrolyzer performance by adding 20% MeCN to the electrolyte, and then measured the E_{cell} for 2-Chamber Electrolyzer again over the 20–80 ºC range (Fig. 4b). Experiments with a H_2O/MeCN (4:1) mixed electrolyte at 60 °C achieved an E_{cell} of 0.38 V at 100 mA cm^{-2}, which was slightly higher than the 0.32 V measured with the aqueous electrolyte at the same temperature.

At higher current densities and 60 ºC, the addition of MeCN in the electrolyte played an important role on electrolyzer performance: At 1 A cm^{-2} the voltage was 4.23 V and 5.03 V with and without MeCN in the electrolyte, respectively (fig. S4c and Table 2).

The effects of pH

We monitored the electrolyte pH as a function of time during each electrolysis experiment. When using a H_2O/MeCN mixed electrolyte for 2-Chamber Electrolyzer, the anolyte and catholyte reached a steady-state pH of 6.3 and 13.2, respectively, after 30 min (Fig. 5a and fig. S12). The high pH of the catholyte enabled rapid precipitation of $Ca(OH)_{2(s)}$ in the Calcium Reactor. The desired $Ca(OH)_{2(s)}$ product for each campaign was confirmed by Fourier-transform infrared (FTIR, fig. S13a) spectroscopy and X-ray diffraction (XRD) measurements (fig. S13b).(*8*, *28*, *29*) Notably, the same experiments with the aqueous electrolyte yielded a lower catholyte pH of 11.8, which proved insufficient for $Ca(OH)_{2(s)}$ precipitation.

https://doi.org/10.26434/chemrxiv-2024-fvxrb ORCID: https://orcid.org/0000-0001-6875-849X Content not peer-reviewed by ChemRxiv. License: CC BY-NC-ND 4.0

Discussion

The PCET chemistry associated with organic redox shuttles(*30*) has proven effective in a range of electrochemical applications, including high-voltage redox flow batteries,(*16–18*) supercapacitors,(*19–21*) and CO_2 capture.(*22–24*) (Hydro)anthraquinones have been particularly effective for their high solubility, fast kinetics, high chemical stability, tunable redox potentials, and low cost.(*15*, *30*)

We identified that the PCET reactions associated with $(H_2)AQ$ could potentially drive the release and uptake of protons in a cement electrolyzer in favorable ways. For example, if the pH could be made sufficiently acidic in the anolyte, the anolyte could be used to convert $CaCO_{3(s)}$ into reactive Ca^{2+} ions. Likewise, a sufficiently caustic catholyte could react with Ca^{2+} ions to form the desired electrochemically upgraded $Ca(OH)_{2(s)}$ product. We were also drawn to the fact that PCET reactions with (hydro)anthraquinones show small differences in redox potentials across a wide range of pH (ΔE^0 at pH 7–14 are typically <0.4 V).(*15*)

It is for these reasons that we built a 3-Chamber Electrolyzer, a reactor analogous to our initial Control Electrolyzer, but with H_2AQ and AQ in the electrolyte. Indeed, the PCET chemistry of $(H_2)AQ$ enabled the E_{cell} to be reduced by 2.6 V relative to the Control Electrolyzer at 100 mA cm^{-2} (Table 1). However, the resultant E_{cell} was still too high. We therefore removed the chemical chamber to construct a zero-gap configuration with only anode and cathode chambers, which yielded yet another massive drop in E_{cell}. These design changes confirmed that the narrow electrochemical window of the (hydro)anthraquinone electrolyte (fig. S2) and the two-chamber cell design collectively reduced the voltage required to drive limestone decomposition at 1.3 V at 100 mA cm^{-2}, and 11.4 V at 1 A cm^{-2}.

These positive results notwithstanding, we encountered issues related to the formation of quinone dimer byproducts. We addressed this solubility issue by both heating the electrolyte, and by adding organic solvents to the electrolyte. We converged on a H_2O/MeCN (4:1) mixed electrolyte system set at 60 °C as the optimal conditions. The higher temperatures benefit cell voltage by

https://doi.org/10.26434/chemrxiv-2024-fvxrb ORCID: https://orcid.org/0000-0001-6875-849X Content not peer-reviewed by ChemRxiv. License: CC BY-NC-ND 4.0

minimizing quinone dimer byproduct formation (fig. S6–10), and also by increasing the diffusion of (H_2)AQ species (fig. S11, tables S2 and S3).(*27*, *31–33*) These experimental modifications had an especially large impact on voltage at high current densities (fig. S4, and table S1).

The formation of quinone is likely suppressed at high temperatures due to the disruption of the intramolecular hydrogen bonding of quinhydrone and quinone.(*27*, *33*) We conjecture that the addition of MeCN to the electrolyte also disrupts hydrogen bonding. This claim is supported by electrolysis experiments with 2-Chamber Electrolyzer, where the H_2O/MeCN mixed electrolyte operates at far lower voltage (4.23 V) than the aqueous electrolyte (5.03 V) at a current density of 1 A cm^{-2}. Moreover, the mixed-solvent electrolyte yielded a more constant voltage during longer electrolysis runs (Fig. 6 and table S1), which was reproducible over successive Cycles (Fig. 5b).

Another important advantage of the mixed-solvent system is that the catholyte becomes more basic during electrolysis: The pH of the MeCN-containing catholyte of 2-Chamber Electrolyzer reached 13.2 after 30 min of electrolysis (Fig. 5a), which is substantially more basic than the pH of 11.78 that can be reached with the purely aqueous system. We attribute the higher pH to MeCN suppressing the dissociation of protons from H_2AQ.(*34*, *35*) This effect is important because the higher pH acts to lower the solubility of the desired $Ca(OH)_{2(s)}$ product, working in our favor for precipitation the desired $Ca(OH)_{2(s)}$ product in the Calcium Reactor. The mixed-solvent system therefore yields superior electrolytic limestone-to-$Ca(OH)_{2(s)}$ conversion than the experiments with aqueous medium.

The 2-Chamber Electrolyzer also yielded a much higher Faradaic efficiency (100%) than the 3-Chamber Electrolyzer (<40%). These significant differences arise from the very different reaction chemistries that occur in the two electrolyzers. When $CaCO_{3(s)}$ enters the 2-Chamber Electrolyzer, it reacts with protons sourced from H_2AQ in the anode chamber. This $CaCO_{3(s)}$ instead reacts with protons delivered from the BPM in the three-chamber configuration.

The $CaCO_{3(s)}$ slurry was also delivered to each of the reactors differently, with very different flow fields. For the 2-Chamber Electrolyzer, $CaCO_{3(s)}$ was delivered through flow channels, while the

https://doi.org/10.26434/chemrxiv-2024-fvxrb ORCID: https://orcid.org/0000-0001-6875-849X Content not peer-reviewed by ChemRxiv. License: CC BY-NC-ND 4.0

3-Chamber Electrolyzer delivered $CaCO_{3(s)}$ into a central chemical chamber lacking any flow channels. The thicknesses of the chemical and anode chambers were held at parity for Electrolyzers A and B, and thus we assert that it is the delivery of the $CaCO_{3(S)}$ slurry through the flow channels and high surface area graphite felt that enables the more efficient reaction between H^+ and $CaCO_{3(s)}$ (Fig. 2 and fig. S3). In contrast, protons released from the BPM cannot react as effectively with $CaCO_{3(s)}$ in the chemical chamber lacking the flow channels. This claim is supported by the fact that the pH of the electrolyte in the chemical chamber of 3-Chamber Electrolyzer was more acidic (pH 5.4) than the anolyte in 2-Chamber Electrolyzer (pH 6.3), and by the higher rate of production of *i*-$CO_{2(g)}$ in 2-Chamber Electrolyzer (fig. S5). It is these design considerations that enabled us to achieve quantitative Faradaic efficiencies with the 2-Chamber Electrolyzer.

We designed and built a 2-Chamber Electrolyzer capable of decomposing limestone $Ca(CO_3)_{(s)}$ under continuous flow with high energy and Faradaic efficiencies. This electrolyzer produces independent product streams from the anode and cathode chambers that can be mixed in an independent reactor to react Ca^{2+} and OH^- ions to form the targeted $Ca(OH)_{2(s)}$ product. This solid product can be isolated and used for downstream processing into cement clinker, while the remaining electrolyte can be delivered back to the cement electrolyzer for successive reaction with limestone feedstock.

The zero-gap two-chamber configuration of this electrolyzer, coupled to the use of organic redox mediators and mixed solvents, enabled limestone decomposition at exceptionally low voltages and with high faradaic efficiency. This electrolyzer provides a viable pathway for decarbonizing cement production.

Acknowledgements

The authors are grateful to the New Frontiers in Research Fund (NFRFT-2022-00197), the Canadian Natural Sciences and Engineering Research Council (RGPIN-2018-06748), Canadian Foundation for Innovation (229288), Canadian Institute for Advanced Research (BSE-BERL-162173), and Canada

https://doi.org/10.26434/chemrxiv-2024-fvxrb **ORCID:** https://orcid.org/0000-0001-6875-849X Content not peer-reviewed by ChemRxiv. **License:** CC BY-NC-ND 4.0

Research Chairs for financial support. This research was undertaken thanks in part to funding from the Canada First Research Excellence Fund, Quantum Materials and Future Technologies Program. Scanning electron microscopy imaging was performed in the Centre for High-Throughput Phenogenomics at the University of British Columbia. The authors thank Dr. Maureen Soon for performing the ICP-OES measurements and Dr. Anita Lam for help in the XRD measurements.

Competing interests

A related PCT patent application has been filed: Berlinguette, C. P.; Zhang, Z.; Mowbray, B. A. W. "Methods and Apparatus for Converting Metal Carbonate Salts to Metal Hydroxides". PCT International Application No. PCT/CA2023/050064, filed January 20 2023. Priority data: US Provisional Patent Application No. 63/301,189, filed January 20 2022. The authors declare no other competing interests.

Author Information

ORCID

Tengxiao Ji 0000-0001-9652-9598

Shaoxuan Ren 000-0003-4875-7558

Gaopeng Jiang 0000-0003-4114-4281

Yongwook Kim 0000-0002-2381-4379

Monika Stolar 0000-0002-2709-2983

Curtis P. Berlinguette 0000-0001-6875-849X

*Corresponding author Email: cberling@chem.ubc.ca

Supplementary Materials

Materials and Methods

Supplementary Text

https://doi.org/10.26434/chemrxiv-2024-fvxrb **ORCID:** https://orcid.org/0000-0001-6875-849X Content not peer-reviewed by ChemRxiv. **License:** CC BY-NC-ND 4.0

Figs. S1 to S13

Tables S1 to S3

References (*1–6*)

Movies S1

References and notes

1. N. Mohamad, K. Muthusamy, R. Embong, A. Kusbiantoro, M. H. Hashim, Environmental impact of cement production and solutions: A review. *Materials Today: Proceedings*. **48**, 741–746 (2022). doi: 10.1016/j.matpr.2021.02.212

2. L. D. Ellis, A. F. Badel, M. L. Chiang, R. J.-Y. Park, Y.-M. Chiang, Toward electrochemical synthesis of cement-An electrolyzer-based process for decarbonating $CaCO_3$ while producing useful gas streams. *Proc. Natl. Acad. Sci. U. S. A.* **117**, 12584–12591 (2020). doi: 10.1073/pnas.1821673116

3. M. Schneider, M. Romer, M. Tschudin, H. Bolio, Sustainable cement production—present and future. *Cem. Concr. Res.* **41**, 642–650 (2011). doi: 10.1016/j.cemconres.2011.03.019

4. I. Galan, C. Andrade, P. Mora, M. A. Sanjuan, Sequestration of CO_2 by concrete carbonation. *Environ. Sci. Technol.* **44**, 3181–3186 (2010). doi: 10.1021/es903581d

5. M. Kazemian, B. Shafei, Carbon sequestration and storage in concrete: A state-of-the-art review of compositions, methods, and developments. *Journal of CO_2 Utilization*. **70**, 102443 (2023). doi: 10.1016/j.jcou.2023.102443

6. M. Pisciotta, H. Pilorgé, J. Davids, P. Psarras, Opportunities for cement decarbonization. *Cleaner Engineering and Technology*. **15**, 100667 (2023). doi: 10.1016/j.clet.2023.100667

7. J. Skibsted, R. Snellings, Reactivity of supplementary cementitious materials (SCMs) in cement blends. *Cem. Concr. Res.* **124**, 105799 (2019). doi: 10.1016/j.cemconres.2019.105799

8. Z. Zhang, B. A. W. Mowbray, C. T. E. Parkyn, C. Waizenegger, A. S. R. Williams, E. W. Lees, S. Ren, Y. Kim, R. P. Jansonius, C. P. Berlinguette, Cement clinker precursor production in an electrolyser. *Energy Environ. Sci.* **15**, 5129–5136 (2022). doi: 10.1039/D2EE02349K

9. B. A. W. Mowbray, Z. B. Zhang, C. T. E. Parkyn, C. P. Berlinguette, Electrochemical cement clinker precursor production at low voltages. *ACS Energy Lett.* **8**, 1772–1778 (2023). doi: 10.1021/acsenergylett.3c00242

10. Q. Xie, L. Wan, Z. Zhang, J. Luo, Electrochemical transformation of limestone into calcium hydroxide and valuable carbonaceous products for decarbonizing cement production. *iScience*. **26**, 106015 (2023). doi: 10.1016/j.isci.2023.106015

11. A. Perego, D. Kulkarni, H.-M. Chang, X. Wang, J. Wei, M. Li, I. V. Zenyuk, Electrochemical flow

https://doi.org/10.26434/chemrxiv-2024-fvxrb **ORCID:** https://orcid.org/0000-0001-6875-849X Content not peer-reviewed by ChemRxiv. **License:** CC BY-NC-ND 4.0

reactor for cement clinker production. *Meet. Abstr.* **MA2021-02**, 840 (2021). doi: 10.1149/MA2021-0227840mtgabs

12. Z. Zhang, B. Mowbray, C. Parkyn, Y. Kim, C. Berlinguette, Electrolytic cement clinker production sustained through orthogonalization of ion vectors. *ChemRxiv* (2023). doi:10.26434/chemrxiv-2023-0zcw9

13. R. K. Miao, N. Wang, S.-F. Hung, W.-Y. Huang, J. Zhang, Y. Zhao, P. Ou, S. Wang, J. P. Edwards, C. Tian, J. Han, Y. Xu, M. Fan, J. E. Huang, Y. C. Xiao, A. H. Ip, H. Liang, E. H. Sargent, D. Sinton, Electrified cement production via anion-mediated electrochemical calcium extraction. *ACS Energy Lett.*, 4694–4701 (2023). doi: 10.1021/acsenergylett.3c01668

14. R. Tyburski, T. Liu, S. D. Glover, L. Hammarström, Proton-coupled electron transfer guidelines, fair and square. *J. Am. Chem. Soc.* **143**, 560–576 (2021). doi: 0.1021/jacs.0c09106

15. K. Wedege, E. Dražević, D. Konya, A. Bentien, Organic redox species in aqueous flow batteries: Redox potentials, chemical stability and solubility. *Sci. Rep.* **6**, 39101 (2016). doi: 10.1038/srep39101

16. A. Orita, M. G. Verde, M. Sakai, Y. S. Meng, A biomimetic redox flow battery based on flavin mononucleotide. *Nat. Commun.* **7**, 13230 (2016). doi: 0.1038/ncomms13230

17. M. Pan, L. Gao, J. Liang, P. Zhang, S. Lu, Y. Lu, J. Ma, Z. Jin, Reversible redox chemistry in pyrrolidinium‐based TEMPO radical and extended viologen for high‐voltage and long‐life aqueous redox flow batteries. *Adv. Energy Mater.* **12**, 2103478 (2022). doi: 10.1002/aenm.202103478

18. E. F. Kerr, Z. Tang, T. Y. George, S. Jin, E. M. Fell, K. Amini, Y. Jing, M. Wu, R. G. Gordon, M. J. Aziz, High energy density aqueous flow battery utilizing extremely stable, branching-induced high-solubility anthraquinone near neutral pH. *ACS Energy Lett.* **8**, 600–607 (2023). doi: 10.1021/acsenergylett.2c01691

19. D. Vonlanthen, P. Lazarev, K. A. See, F. Wudl, A. J. Heeger, A stable polyaniline-benzoquinone-hydroquinone supercapacitor. *Adv. Mater.* **26**, 5095–5100 (2014). doi: 10.1002/adma.201400966

20. W. Chen, R. B. Rakhi, H. N. Alshareef, Capacitance enhancement of polyaniline coated curved-graphene supercapacitors in a redox-active electrolyte. *Nanoscale*. **5**, 4134–4138 (2013). doi: 10.1039/C3NR00773A

21. J. Liu, Y. Yuan, H. Fang, Y. Xu, W. Sun, S. Chen, Y. Wang, L.-P. Lv, Redox-active tetramino-benzoquinone π–π stacking and H-bonding onto multiwalled carbon nanotubes toward a high-performance asymmetric supercapacitor. *ACS Appl. Energy Mater.* **5**, 8112–8122 (2022). doi: 10.1021/acsaem.2c00627

22. S. Jin, M. Wu, R. G. Gordon, M. J. Aziz, D. G. Kwabi, pH swing cycle for CO_2 capture electrochemically driven through proton-coupled electron transfer. *Energy Environ. Sci.* **13**, 3706–3722 (2020). doi: 10.1039/D0EE01834A

23. S. Jin, M. Wu, Y. Jing, R. G. Gordon, M. J. Aziz, Low energy carbon capture via electrochemically induced pH swing with electrochemical rebalancing. *Nat. Commun.* **13**, 2140 (2022). doi:

https://doi.org/10.26434/chemrxiv-2024-fvxrb **ORCID:** https://orcid.org/0000-0001-6875-849X Content not peer-reviewed by ChemRxiv. **License:** CC BY-NC-ND 4.0

10.1038/s41467-022-29791-7

24. S. Pang, S. Jin, F. Yang, M. Alberts, L. Li, D. Xi, R. G. Gordon, P. Wang, M. J. Aziz, Y. Ji, A phenazine-based high-capacity and high-stability electrochemical CO_2 capture cell with coupled electricity storage. *Nature Energy*. **8**, 1126–1136 (2023). doi: 10.1038/s41560-023-01347-z

25. D. A. Salvatore, D. M. Weekes, J. He, K. E. Dettelbach, Y. C. Li, T. E. Mallouk, C. P. Berlinguette, Electrolysis of gaseous CO_2 to CO in a flow cell with a bipolar membrane. *ACS Energy Lett.* **3**, 149–154 (2018). doi: 10.1021/acsenergylett.7b01017

26. D. M. Weekes, D. A. Salvatore, A. Reyes, A. Huang, C. P. Berlinguette, Electrolytic CO_2 reduction in a flow cell. *Acc. Chem. Res.* **51**, 910–918 (2018). doi: 10.1021/acs.accounts.8b00010

27. T. J. Carney, S. J. Collins, J. S. Moore, F. R. Brushett, Concentration-dependent dimerization of anthraquinone disulfonic acid and its impact on charge storage. *Chem. Mater.* **29**, 4801–4810 (2017). doi: 10.1021/acs.chemmater.7b00616

28. A. L. Zhu, D. Duch, G. A. Roberts, S. X. X. Li, H. Wang, K. Duch, E. Bae, K. S. Jung, D. Wilkinson, S. A. Kulinich, Increasing the electrolyte capacity of alkaline Zn-air fuel cells by scavenging zincate with $Ca(OH)_2$. *ChemElectroChem*. **2**, 134–142 (2015). doi: 10.1002/celc.201402251

29. Z. Liang, Q. Wang, B. Dong, B. Jiang, F. Xing, Ion-triggered calcium hydroxide microcapsules for enhanced corrosion resistance of steel bars. *RSC Adv.* **8**, 39536–39544 (2018). doi: https://doi.org/10.1039/C8RA07382A

30. M. Pan, M. Shao, Z. Jin, Development of organic redox‐active materials in aqueous flow batteries: Current strategies and future perspectives. *SmartMat*. **4** (2023). doi:10.1002/smm2.1198

31. C. Wiberg, T. J. Carney, F. Brushett, E. Ahlberg, E. Wang, Dimerization of 9,10-anthraquinone-2,7-disulfonic acid (AQDS). *Electrochim. Acta*. **317**, 478–485 (2019). doi: 10.1016/j.electacta.2019.05.134

32. L. Tong, Q. Chen, A. A. Wong, R. Gómez-Bombarelli, A. Aspuru-Guzik, R. G. Gordon, M. J. Aziz, UV-vis spectrophotometry of quinone flow battery electrolyte for in situ monitoring and improved electrochemical modeling of potential and quinhydrone formation. *Phys. Chem. Chem. Phys.* **19**, 31684–31691 (2017). doi: 10.1039/C7CP05881K

33. P. Mazúr, J. Charvát, J. Mrlík, J. Pocedič, J. Akrman, L. Kubáč, B. Řeháková, J. Kosek, Evaluation of electrochemical stability of sulfonated anthraquinone-based acidic electrolyte for redox flow battery application. *Molecules*. **26** (2021). doi:10.3390/molecules26092484

34. P. D. Astudillo, J. Tiburcio, F. J. González, The role of acids and bases on the electrochemical oxidation of hydroquinone: Hydrogen bonding interactions in acetonitrile. *J. Electroanal. Chem.* **604**, 57–64 (2007). doi: 10.1016/j.jelechem.2007.02.031

35. L. E. Friedrich, The two hydrogen-oxygen bond-dissociation energies of hydroquinone. *J. Org. Chem.* **48**, 3851–3852 (1983). doi: 10.1021/jo00169a062

https://doi.org/10.26434/chemrxiv-2024-fvxrb **ORCID:** https://orcid.org/0000-0001-6875-849X Content not peer-reviewed by ChemRxiv. **License:** CC BY-NC-ND 4.0

https://doi.org/10.26434/chemrxiv-2024-fvxrb **ORCID:** https://orcid.org/0000-0001-6875-849X Content not peer-reviewed by ChemRxiv. **License:** CC BY-NC-ND 4.0